 https://doi.org/10.3311/PPee.21852


**Periodica Polytechnica Electrical Engineering and Computer Science**, 67(3), pp. 268–280, 2023

# Backstepping Based Grey Wolf and DPC for Power Quality Improvement and Active Power Injection in PV Grid-connected System Based on Interleaved Boost Converter

Oussama Mohamed Cherif Daia Eddine[1], Ali Chebabhi[2], Abdelhalim Kessal[1*]

[1] LPMRN Laboratory, Faculty of Sciences & Technology, University Mohammed El Bachir El Ibrahimi of Bordj Bou Arreridj, 34030 Bordj Bou Arreridj, P.O.B. 64, Algeria
[2] EE Laboratory, Department of Electrical Engineering, Faculty of Technology, University of M'sila, 28000 M'sila, P.O.B. 166, Algeria
[*] Corresponding author, e-mail: abdelhalim.kessal@univ-bba.dz

Received: 13 January 2023, Accepted: 27 April 2023, Published online: 25 May 2023

**Abstract**

This research offers the backstepping based grey wolf control design for a multifunctional PV grid-connected system (MPGC) based on four phases interleaved boost converter. This work proposes a solution to the issues of harmonic mitigation, reactive power compensation, and PV-generated power injection into the grid-based MPGC. The interleaved boost converter (IBC), controlled using maximum power point tracking (MPPT), is utilized to harvest the photovoltaic (PV) system's peak power and overcome the conventional topology's drawbacks. Direct power control (DPC) based on space-vector pulse width modulation (SVPWM) is used to control the instantaneous power of the MPGC, and the backstepping control (BSC) is applied to the whole system to maintain the robustness and stability of the suggested method. The Grey Wolf Optimizer (GWO) optimized the system's dynamic response by adjusting the BSC parameters. The results were obtained using MATLAB/Simulink software. The suggested work shows excellent performance based on the obtained results, achieving the sinusoidal waveform of the currents and a unity power factor. Total harmonic distortion (THD) has been decreased below 5% in accordance with IEEE 519-2014 standard.

**Keywords**

grid-connected, photovoltaic, backstepping control, Grey Wolf Optimizer, interleaved boost converter

## 1 Introduction

Wind, solar, geothermal, and biomass energy are a few examples of renewable energy sources that are gaining popularity as an alternative to fossil fuels. PV systems are among the most rapidly expanding renewable energy sources due to their lack of emissions, low cost, unlimited availability, and widespread distribution [1]. Meanwhile, nonlinear loads are used in many applications and power electronic devices, such as voltage source inverters and adjustable speed drivers (ASD). It damages the distribution grid current due to reactive power consumption, power factor retraction, and injecting harmonic currents into the grid [2, 3].

Interconnecting photovoltaic (PV) systems with the power grid are one of the essential functions that multifunctional PV grid-connected systems (MPGC) provide for distributed generating grids, harmonics mitigation, and reactive power compensation to achieve unity power factor [4]. The MPGC typically features a two-stage power conversion scheme. The highest DC power possible from the PV system is provided in the first stage, generally using DC-DC boost converters. In contrast, this DC power is transported to the grid by converting it to AC power in the second stage, using PWM inverters [5]. The PWM inverter is generally used as a shunt active-power filter (SAPF) to reduce harmonic current, compensate for reactive power, and insert PV-generated energy into the main grid [6].

The solar panels are usually coupled with a DC-DC boost converter to raise their voltage and bring it up to the desired level by the DC link voltage. Moreover, it maintains the PV power close to the peak power using a maximum power point tracker (MPPT) controller. However, due to its benefits, which include low power ripple, high efficiency, a small size, and suitability for high-power applications, the interleaved boost converter is a topology utilized to avoid the restrictions inherent to the conventional boost converter [7, 8].

**Cite this article as:** Daia Eddine, O. M. C., Chebabhi, A., Kessal, A. "Backstepping Based Grey Wolf and DPC for Power Quality Improvement and Active Power Injection in PV Grid-connected System Based on Interleaved Boost Converter", Periodica Polytechnica Electrical Engineering and Computer Science, 67(3), pp. 268–280, 2023. https://doi.org/10.3311/PPee.21852

Generally, each stage of the MPGC structure consists of two control loops: the PV voltage and inductor current control loops in the first stage (PV-IBC) and the DC bus voltage and grid power control loops in the second stage (SAPF). When the direct power control (DPC) method is used for controlling the SAPF. As a result, there is a power coupling between both stages on the one hand and between them and the grid on the other, which means that the disturbances of one loop affect the overall system.

On the other hand, the control performance and dynamic response of the MPGC system depend strongly on the selected controllers in whole control loops. The multiple linear and nonlinear control techniques developed for MPGC based on IBC have the same purpose with various functionalities [8]. Linear controllers such as proportional integral controllers (PICs) have been proposed to achieve excellent steady-state performance and dynamic response [9]. Chettibi and Mellit [10] proposes a PI controller-based DPC-SVPWM strategy. Moreover, PSO is used to tune the DC bus voltage controller. However, the DC bus voltage behavior shows a high overshoot, a considerable settling time, and a high-power ripple. In addition, the inherent nonlinearities of the MPGC based on IBC and the undesirable perturbations due to parameters variation affecting its dynamics will not only impact its performance and stability but also lead to poor dynamic responses in transient states.

To further improve the control performance and dynamic responses of the MPGC system and to overcome the PI controller's issues and weaknesses, several advanced nonlinear control techniques have been proposed for controlling the MPGC systems in recent years. In [11], sliding mode control (SMC) based DPC-SVPWM is proposed to control the MPGC system, which shows superior control performance and dynamic responses over the PI controller. Furthermore, SMC rejects external disturbances and exhibits robust performance versus variation of the system parameters. The main limitation of this control technique is the chattering phenomenon, which causes power loss and overheating of power switches.

Various papers propose a nonlinear backstepping technique (BSC) to overcome the SMC limitations and further improve the control performance and dynamic responses of distributed resource systems based on renewable energy [12], grid-connected power converters [13], and machine drives [14] have been recognized as an effective technique due to its benefits of recursive design, high robustness, and good performance under different operating scenarios. These factors have led to the BSC's widespread adoption in control of distributed resource systems that rely on renewable energy and grid-connected power converters [15–18]. Chebabhi et al. [15] proposed a BSC to control the DC bus voltage and output currents of SAPF. Naghmash et al. [16] proposed a BSC for MPPT in a photovoltaic system. Martin et al. [17] proposed a BSC for a smart grid-connected photovoltaic power system based on a conventional DC-DC boost converter for telecom equipment. Hao et al. [18] investigated the BSC for the inner loop of four-phase IBC-based proton exchange membrane fuel cells.

Furthermore, the BSC-based DPC-SVPWM technique was investigated for a grid-connected photovoltaic system based on a conventional DC-DC boost converter to control the instantaneous active/reactive power and DC bus voltage simultaneously [19]. The obtained results confirm the superiority and effectiveness of BSC compared with the PICs in terms of rapidity, stability, harmonic mitigation, reactive power compensation, PV-generated power injection, and robustness. However, because all real-world systems are susceptible to change over time and there are many regulators in the overall system, it is not practical to constantly redesign the system and the regulators. These changes cause steady-state output errors, which reduce the regulator’s effectiveness. Consequently, the large power ripple in the case of a conventional DC-DC boost converter is not considered; the high-power quality cannot be ensured when this converter is used.

This paper proposes a DPC-SVPWM based on backstepping control to control the MPGC system. The four-leg interleaved boost converter is adopted in this work for its benefits, which include low power ripple, high efficiency, a small size, and suitability for high-power applications [20, 21]. To reduce the steady-state error in the DC bus voltage of the MPGC, a BSC with integral action (IBSC) with an anti-windup compensator has been used. The proposed BSC and IBSC controller parameters are calculated using the Grey Wolf Optimization (GWO) algorithm to obtain a fast response time, zero steady-state error, low overshoot, and reduced power ripple. The paper's objectives are:

- to inject the power of the PV system into the grid;
- compensate the reactive power to guarantee the power factor unity;
- current harmonics mitigation that is generated from nonlinear loads;
- eliminate the drawbacks of the CBC by using an IBC topology;

- optimize the BS controller to overcome the nonlinear behavior of the system, ensure its robustness and stability, and enhance its performance.

## 2 System descriptions

The MPGC configuration comprises a three-phase inverter connected to a three-phase grid network across three inductors, $L_{S1}$, $L_{S2}$, and $L_{S3}$. The inverter DC side is associated in parallel with a capacitor supplied by an interleaved boost converter-based PV system. In addition, an uncontrolled three-phase rectifier with an RL charge is regarded as a nonlinear load connected to the grid. Fig. 1 depicts the system's structure under study.

Four legs interleaved boost converter [20, 21] is an enhanced boost converter used to overcome the CBC drawbacks. It consists of four CBCs connected in parallel to the same input and output and uses a pulse width modulation block with a 90° phase shift between their carrier signals. In Fig. 2, the FLIBC circuit has been presented.

## 3 Control approach

### 3.1 Direct power control-based backstepping technique

DPC-SVPWM is an enhanced version of the classical DPC proposed to eliminate its drawbacks and permit it to operate at a fixed switching frequency. The comparators and switching table are replaced with regulators and a space vector pulse width modulation block. The SVPWM is used in the final step of DPC to generate the modulated signals ($S_a$, $S_b$, and $S_c$) for the PWM inverter switches based SAPF to generate the desired output voltages to the grid, as illustrated in Fig. 3.

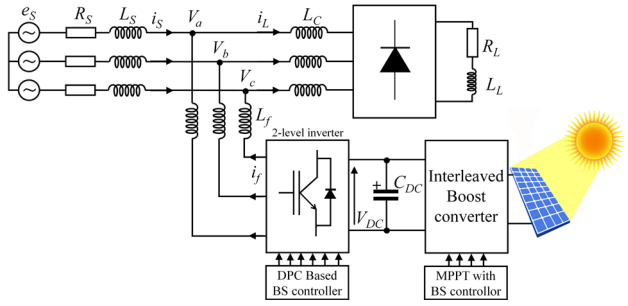


**Fig. 1** Multifunctional grid-connected PV system-based IBC

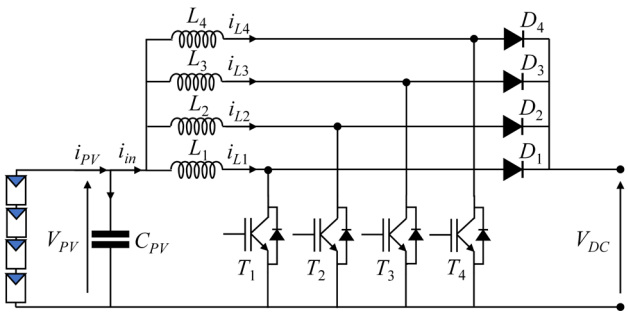


**Fig. 2** Four phases interleaved boost converter connected to PV panels

By using Kirchhoff's law and the stationary frame, the deferential equation that describes the dynamics of the three-phase two-level inverter can be obtained as follows:

$$L_f \frac{di}{dt} = -R_f i + U_{fx} - V_x, \quad x = \alpha, \ \beta, \tag{1}$$

where $V_x$ is the point of common coupling voltage ($V_{PCC}$), $i_f$ is the inverter current, and $U_f$ is the inverter output voltage.

The active power reference is delivered using an external control loop-based BS controller of the DC bus voltage controller. The reactive power set point equals zero to guarantee unity power factor operation [22]. According to instantaneous reactive power theory, the grid's instantaneous powers in a stationary reference frame can be expressed as:

$$\begin{cases} P = V_{s\alpha} i_{s\alpha} + V_{s\beta} i_{s\beta} \\ Q = V_{s\beta} i_{s\alpha} - V_{s\alpha} i_{s\beta} \end{cases}, \tag{2}$$

where $V_s$ and $i_s$ are the source voltage and current, respectively.

To design the backstepping controller of the MPGC, we need to use Eq. (1). Then, rewrite Eq. (1) as follows:

$$L_f \begin{bmatrix} \frac{di_\alpha}{dt} \\ \frac{di_\beta}{dt} \end{bmatrix} = -R_f \begin{bmatrix} i_\alpha \\ i_\beta \end{bmatrix} - \begin{bmatrix} V_\alpha \\ V_\beta \end{bmatrix} + \begin{bmatrix} U_{f\alpha} \\ U_{f\beta} \end{bmatrix}. \tag{3}$$

Subsequently, the differential equation that describes the behavior of the instantaneous power of the MPGC can be obtained using Eqs. (2) and (3) as:

$$L_f \begin{bmatrix} \dot{P} \\ \dot{Q} \end{bmatrix} = -R_f \begin{bmatrix} P \\ Q \end{bmatrix} + \begin{bmatrix} V_\alpha & V_\beta \\ V_\beta & -V_\alpha \end{bmatrix} \left( \begin{bmatrix} U_{f\alpha} \\ U_{f\beta} \end{bmatrix} - \begin{bmatrix} V_\alpha \\ V_\beta \end{bmatrix} \right). \tag{4}$$

We can rewrite Eq. (4) as follows:

$$L_f \begin{bmatrix} \dot{P} \\ \dot{Q} \end{bmatrix} = -R_f \begin{bmatrix} P \\ Q \end{bmatrix} + \begin{bmatrix} u_{f\alpha} \\ u_{f\beta} \end{bmatrix}, \tag{5}$$

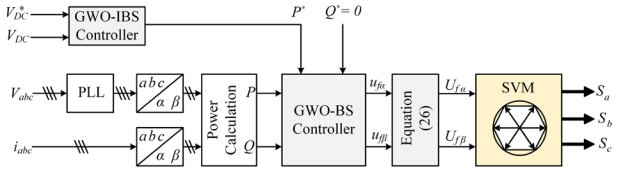


**Fig. 3** Direct power control with SVPWM-based GWO-BS scheme

where:

$$\begin{bmatrix} u_{f\alpha} \\ u_{f\beta} \end{bmatrix} = \begin{bmatrix} V_\alpha & V_\beta \\ V_\beta & -V_\alpha \end{bmatrix} \left( \begin{bmatrix} U_{f\alpha} \\ U_{f\beta} \end{bmatrix} - \begin{bmatrix} V_\alpha \\ V_\beta \end{bmatrix} \right). \tag{6}$$

The DPC-SVPWM can directly control the active and reactive power thanks to the control $u_{f\alpha}$ and $u_{f\beta}$. The power loop's control law is derived from the Lyapunov function. The tracking errors are defined as:

$$\begin{cases} e_1 = P^* - P \\ e_2 = Q^* - Q \end{cases}. \tag{7}$$

Their time derivatives:

$$\begin{cases} \dot{e}_1 = \dot{P}^* - \dot{P} = \dot{P}^* + \dfrac{R_f}{L_f} P - \dfrac{u_{f\alpha}}{L_f} \\ \dot{e}_2 = \dot{Q}^* - \dot{Q} = \dot{Q}^* + \dfrac{R_f}{L_f} Q - \dfrac{u_{f\beta}}{L_f} \end{cases}. \tag{8}$$

The Lyapunov functions are selected as follows:

$$\begin{cases} V_1 = \dfrac{1}{2} e_1^2 \\ V_2 = \dfrac{1}{2} e_2^2 \end{cases}. \tag{9}$$

Their time derivatives are represented as:

$$\begin{cases} \dot{V}_1 = e_1 \dot{e}_1 \\ \dot{V}_2 = e_2 \dot{e}_2 \end{cases}. \tag{10}$$

The time derivatives of Lyapunov functions should be negative definite to ensure the system's stability, where $\dot{V}_1 < 0$ and $\dot{V}_2 < 0$. For that, let's assume:

$$\begin{cases} \dot{V}_1 = \dot{e}_1 e_1 = -K_1 e_1^2 \\ \dot{V}_2 = \dot{e}_2 e_2 = -K_2 e_2^2 \end{cases}, \tag{11}$$

where $K_1$ and $K_2$ are definite positive constants. According to Eq. (11), the tracking error Eq. (8)'s time derivative is written as:

$$\begin{cases} \dot{e}_1 = \dot{P}^* + \dfrac{R_f}{L_f} P - \dfrac{u_{f\alpha}}{L_f} = -K_1 e_1 \\ \dot{e}_2 = \dot{Q}^* + \dfrac{R_f}{L_f} Q - \dfrac{u_{f\beta}}{L_f} = -K_2 e_2 \end{cases}. \tag{12}$$

Therefore, from Eq. (12), the control lows $u_{f\alpha}$ and $u_{f\beta}$ can be deduced:

$$\begin{cases} u_{f\alpha} = L_f \left( \dot{P}^* + \dfrac{R_f}{L_f} P + K_1 e_1 \right) \\ u_{f\beta} = L_f \left( \dot{Q}^* + \dfrac{R_f}{L_f} Q + K_2 e_2 \right) \end{cases}. \tag{13}$$

The inverter output voltage $U_f$ can be deduced using Eqs. (6) and (13):

$$\begin{bmatrix} U_{f\alpha} \\ U_{f\beta} \end{bmatrix} = \begin{bmatrix} V_\alpha \\ V_\beta \end{bmatrix} + \frac{1}{V_\alpha^2 + V_\beta^2} \begin{bmatrix} u_{f\alpha} V_\alpha + u_{f\beta} V_\beta \\ u_{f\alpha} V_\beta - u_{f\beta} V_\alpha \end{bmatrix}. \tag{14}$$

### 3.2 DC bus voltage controller design

The operation of the DC bus voltage is described by the differential equation (Eq. (15)), which is written as:

$$\dot{V}_{\mathrm{DC}} = \frac{P}{C_{\mathrm{DC}} V_{\mathrm{DC}}}. \tag{15}$$

The tracking error among the desired DC bus voltage and its measured value has been established to design the controller that provides the active power reference. The nonlinear backstepping controller allows the DC bus voltage to be at the desired value. Integral action is used to eliminate the steady-state error. Whereas the tracking error equations are expressed as:

$$\begin{cases} e_3 = V_{\mathrm{DC}}^* - V_{\mathrm{DC}} \\ e_4 = \int e_3 dt \end{cases}. \tag{16}$$

The Lyapunov function can be represented as follows:

$$V_3 = \frac{1}{2} e_3 + \frac{\delta_3}{2} e_4, \tag{17}$$

where $\delta_3$ is a positive definite constant, the time derivative of $V_3$ can therefore be defined as follows (Eq. (18)):

$$\dot{V}_3 = e_3 \dot{e}_3 + \delta_3 e_4 \dot{e}_4. \tag{18}$$

Equation (18) can be rewritten as:

$$\dot{V}_3 = e_3 \left( \dot{e}_3 + \delta_3 e_4 \right). \tag{19}$$

The time derivative of $V_3$ must be negative for system stability ($\dot{V}_3 < 0$). The Lyapunov function can be expressed as:

$$\dot{V}_3 = -K_3 e_3^2, \tag{20}$$

where $K_3$ is a positive definite constant.

According to Eqs. (19) and (20), we can deduce that:

$$-K_3 e_3 = \dot{e}_3 + \delta_3 e_4. \tag{21}$$

While Eq. (21) can be rewritten as:

$$-K_3 e_3 = \left(\dot{V}_{\mathrm{DC}}^* - \dot{V}_{\mathrm{DC}}\right) + \delta_3 e_4. \tag{22}$$

From Eqs. (22) and (15), the control law $P^*$ can be deduced as:

$$P^* = C_{\mathrm{DC}} V_{\mathrm{DC}} \left(\dot{V}_{\mathrm{DC}}^* + K_3 e_3 + \delta_3 e_4\right). \tag{23}$$

A second integrator term includes an anti-windup loop [23], with a loop gain ($G_3$) adjusted excessively high without impacting the intended performances to prevent the controller's output from being saturated because of the amplification of noise detection. Fig. 4 depicts the DC bus voltage controller with anti-windup back-calculation.

### 3.3 MPPT control algorithm

Numerous MPPT algorithms are utilized to optimize the performance of the PV system [24, 25]. The most widely used and popular technique is perturb and observe (P&O) [26]. The features of this technique are that it is easy to implement and doesn't necessitate the characteristics of the PV generator or the measurement of solar irradiation and cell temperature [27]. The P&O flowchart is represented in Fig. 5. The first step is measuring the panel voltage and current. The second step is calculating the panels' power and the voltage change. Then compare the results with the previous values to select the direction of the next perturbation.

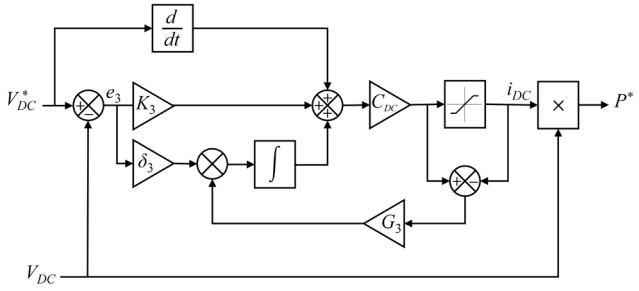


**Fig. 4** Block diagram of DC bus voltage controller

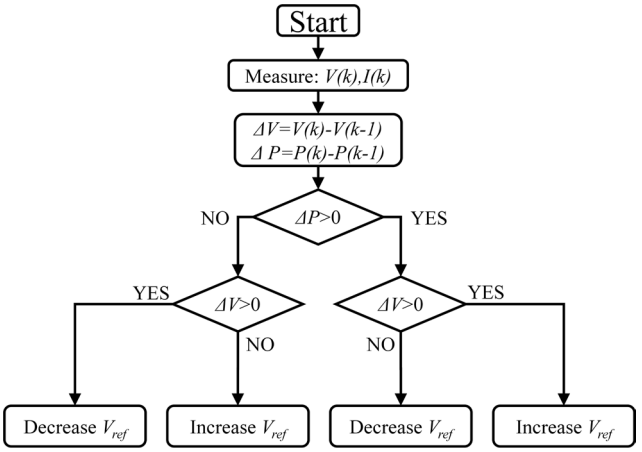


**Fig. 5** The flowchart of the P&O method

### 3.4 Backstepping control of IBC

The modelling of the converter is important for controller design. The circuit diagram of the IBC presented in Fig. 2 functioned in continuous conduction mode, where $V_{PV}$ and $i_{Lj}$ are indicated as the state variables.

When the switch $T_{1,2,3,4}$ is ON, the converter dynamics can be written as:

$$\begin{cases} C_{PV} \dfrac{dV_{PV}}{dt} = i_{PV} - i_{in} \\ L \dfrac{di_{Lj}}{dt} = V_{PV} \end{cases}, \tag{24}$$

where $L = L_{1,2,3,4}$. When the switch $T_{1,2,3,4}$ is OFF, the converter dynamics can be given as:

$$\begin{cases} C_{PV} \dfrac{dV_{PV}}{dt} = i_{PV} - i_{in} \\ L \dfrac{di_{Lj}}{dt} = V_{PV} - V_{\mathrm{DC}} \end{cases}. \tag{25}$$

Therefore, the average dynamic equations of IBC can be written as:

$$\begin{cases} C_{PV} \dfrac{dV_{PV}}{dt} = i_{PV} - i_{in} \\ L \dfrac{di_{Lj}}{dt} = V_{PV} - \left(1 - D_j\right) V_{\mathrm{DC}} \end{cases}, \tag{26}$$

where $D_j \in [0, 1]$ is the duty ratio of each leg.

An integral backstepping controller is designed to reduce voltage tracking errors by adjusting the duty ratio ($D_j$). Let's consider the tracking errors of PV voltage as follows:

$$\begin{cases} e_5 = \left(V_{PV}^* - V_{PV}\right) \\ e_6 = \int e_5 dt \end{cases}. \tag{27}$$

In Eq. (28), the Lyapunov function $V_4$ is selected as:

$$V_4 = \frac{1}{2} e_5^2 + \frac{\delta_6}{2} e_6^2, \tag{28}$$

where $\delta_6$ is a positive definite constant.

The time derivative of the Lyapunov function must be negative definite to maintain the system's asymptotic stability ($\dot{V}_4 < 0$):

$$\dot{V}_4 = e_5 \dot{e}_5 + \delta_6 e_6 \dot{e}_6 = e_5 \left(\dot{e}_5 + \delta_6 e_6\right). \tag{29}$$

Using Eqs. (27) and (29), we get:

$$\dot{V}_4 = e_5 \left(\dot{V}_{PV}^* - \dot{V}_{PV} + \delta_6 e_6\right). \tag{30}$$

For $\dot{V}_4$ be a negative definite, let's assume that:

$$\dot{V}_{PV}^{*} - \dot{V}_{PV} + \delta_6 e_6 = -K_5 e_5, \tag{31}$$

where $K_4$ is a positive definite constant. Therefore, $\dot{V}_4$ becomes:

$$\dot{V}_4 = -K_5 e_5^2. \tag{32}$$

Using Eqs. (26) and (31) can be written as:

$$\frac{1}{C_{PV}}\left(i_{PV} - i_{in}\right) = \dot{V}_{PV}^{*} + K_5 e_5 + \delta_6 e_6. \tag{33}$$

Rewriting Eq. (33) as follows:

$$i_{in} = i_{PV} - C_{PV}\left(\dot{V}_{PV}^{*} + K_5 e_5 + \delta_6 e_6\right). \tag{34}$$

To ensure the current equal sharing among legs, let's consider $\lambda$ as a reference and its mathematical expression written as follows:

$$\lambda = \frac{i_{in}}{4} = \frac{1}{4}\left[i_{PV} - C_{PV}\left(\dot{V}_{PV}^{*} + K_5 e_5 + \delta_6 e_6\right)\right]. \tag{35}$$

Another tracking error is defined for the inductor's current control loop as:

$$e_{7j} = \lambda - i_{Lj}. \tag{36}$$

And the Lyapunov function is given as:

$$V_{5j} = \frac{1}{2} e_{7j}^2. \tag{37}$$

With a negative definite derivative, the Lyapunov function guarantees that the system will remain stable.

$$\dot{V}_{5j} = e_{7j}\dot{e}_{7j}. \tag{38}$$

$\dot{V}_5$ to be negatively definite, let:

$$e_{7j} = -K_{7j} e_{7j}, \tag{39}$$

where $K_{7j}$ is a positive definite constant. Therefore, Eq. (36) becomes:

$$\dot{V}_{5j} = -K_{7j} e_{7j}^2. \tag{40}$$

Using Eqs. (26) and (36), Eq. (39) can be rewritten as follows:

$$\dot{\lambda} - \frac{1}{L}\left[V_{PV} - \left(1 - D_j\right)V_{\mathrm{DC}}\right] = -K_{7j} e_{7j}. \tag{41}$$

Therefore, the control law of each leg can be deduced from Eq. (41) as follows (Eq. (42)):

$$D_j = 1 + \frac{V_{PV}}{V_{\mathrm{DC}}} - \frac{L}{V_{\mathrm{DC}}}\left(\dot{\lambda} + K_{7j} e_{7j}\right). \tag{42}$$

### 3.5 Grey Wolf Optimizer

The Grey Wolf Optimizer (GWO) [28] is a bio-inspired method that mimics the hunting behavior of the grey wolf group. Generally, the group size ranges from 5 to 12 wolves [29]. The hierarchical system of There are four tiers in the grey wolf social hierarchy: alpha ($\alpha$), beta ($\beta$), delta ($\delta$), and omega ($\omega$), where alpha is the leader level, and the three lower levels must follow it. The second-level beta can provide feedback and help the alpha-level make decisions. In addition, lead the two lower levels. The delta level dominates the lowest omega and submits to the alpha and beta levels. The rest wolves are the last level of omega, and they are not important in the group but are required to protect the dominant structure.

Muro et al. [30] describe the principal steps of grey wolf hunting behavior, which are as follows:

1. Approaching, tracking, and pursuing the prey.
2. Pursuit, harass, and encircling maneuver, tracking, and hunting the prey.
3. Attack and hunt the prey.

The following mathematical equations (Eqs. (43) and (44)) describe the procedures mentioned above:

$$\vec{D} = \left|\vec{C} \times \vec{X}_p(i) - \vec{X}(i)\right|, \tag{43}$$

$$\vec{X}(i+1) = \left|\vec{X}_P(i) - \vec{A} \times \vec{D}\right|, \tag{44}$$

where $\vec{X}_P$ is the position vector of the prey, $i$ is the recent iteration, $\vec{X}$ is the vector of the grey wolves' position, $\vec{D}$ is a vector that refers to the distance between the prey and wolves. $\vec{A}$ and $\vec{C}$ are coefficient vectors that can be computed using Eqs. (45) and (46):

$$\vec{C} = 2\vec{r}_1, \tag{45}$$

$$\vec{A} = 2\vec{a}\vec{r}_2 - \vec{a}, \tag{46}$$

whereas $r_1$ and $r_2$ are random numbers that vary in each iteration among the range [0, 1]. In addition, $\vec{a}$ is a vector decreased during iterations from 2 to 0. According to the grey level, the distance of each level can be given as:

$$\begin{cases} \vec{D}_\alpha = \left|\vec{C}_1 \times \vec{X}_\alpha - \vec{X}\right| \\ \vec{D}_\beta = \left|\vec{C}_2 \times \vec{X}_\beta - \vec{X}\right|, \\ \vec{D}_\delta = \left|\vec{C}_3 \times \vec{X}_\delta - \vec{X}\right| \end{cases} \tag{47}$$

where $D_\alpha$, $D_\beta$, and $D_\delta$ are the distances between wolves of alpha level and prey, wolves of beta level and prey, and wolves of delta level and prey. $\vec{C}_1$, $\vec{C}_2$ and $\vec{C}_3$ are the

coefficient vectors of the first three best fittest positions $X_1$, $X_2$, and $X_3$. And $X_\alpha$, $X_\beta$, and $X_\delta$ are the best search agents.

The three best positions of grey wolves are expressed in Eq (48) as:

$$\begin{cases} \vec{X}_1 = \vec{X}_\alpha - \vec{A}_1\left(\vec{D}_\alpha\right) \\ \vec{X}_2 = \vec{X}_\beta - \vec{A}_2\left(\vec{D}_\beta\right), \\ \vec{X}_3 = \vec{X}_\delta - \vec{A}_3\left(\vec{D}_\delta\right) \end{cases} \tag{48}$$

The formula below can be used to compute the position of the prey for the best search agent.

$$\vec{X}\left(i+1\right) = \frac{\vec{X}_1 + \vec{X}_2 + \vec{X}_3}{3}. \tag{49}$$

The pseudo-code of GWO is presented in Algorithm 1.

## 4 Simulation results

The proposed system has been investigated in a simulation developed using MATLAB/Simulink software [31]. Numerous simulation tests have been verified under various operating conditions to prove the performance of the proposed scheme. The simulation results of MPGC based on an IBC controlled using GWO-BS have been compared with those obtained using a PI controller. The simulation and GWO-BS controller parameters are listed in Tables 1 and 2, respectively.

Fig. 6 depicts the waveform and spectrum of the source current before the insertion of the MPGC. The source current is highly deformed, and its total harmonic distortion (THD) value equals 24.74%. Firstly, the proposed system will be examined when the PV panels are disconnected. The aim is to demonstrate their performances in harmonic mitigation, reactive power compensation, and PV power

**Algorithm 1** GWO pseudo-code

1. Initialize the population of the GW $X_i$ ($i$ = 1, 2, …, $n$).
2. Initialize a, A, C.
3. Define each search agent's fitness function. Set $X_\alpha$, $X_\beta$, and $X_\delta$ as the best, the second best, and the third best search agent, respectively.
4. While ($i$ < max iteration).
5. Update the position of each search agent using Eq. (49).
6. Update a, A, C.
7. Calculate each search agent's fitness function.
8. Update $X_\alpha$, $X_\beta$ and $X_\delta$.
9. Set $i = i + 1$.
10. End While.
11. Return $X_\alpha$.

**Table 1** Simulation parameters

| MPGC parameters | | PV panels rated power | |
|---|---|---|---|
| Parameter | Value | Irradiation | Power |
| Source voltage $V_{max}$ | 57 V | 200 W/m² | 206 W |
| Source frequency | 50 Hz | 400 W/m² | 417 W |
| $R_S$, $L_S$ | 0.45 Ω, 2.5 mH | 1000 W/m² | 1022 W |
| $R_f$, $L_f$ | 0.6 Ω, 4 mH | IBC parameters | |
| $R_c$, $L_c$ | 0.6 Ω, 1 mH | L | 8 mH |
| $R_L$, $L_L$ | 16 Ω, 1 mH | Switching frequency | 10 KHz |
| $C_{DC}$ | 1100 µF | | |
| DC bus voltage $V_{DC}$ | 160 V | CPV | 100 uF |

**Table 2** GWO-BS controller parameters

| GWO-BS controller | Parameter value |
|---|---|
| Power controller | $K_1$ = 10 × 107 |
| | $K_2$ = 10 × 107 |
| DC bus controller | $K_3$ = 185.3369 |
| | $\delta_3$ = 7786.4 |
| | $G_3$ = 1469.5 |
| IBC controller | $K_5$ = 44.46 × 106 |
| | $K_7$ = 4 × 104 |
| | $\delta_6$ = 3 × 104 |

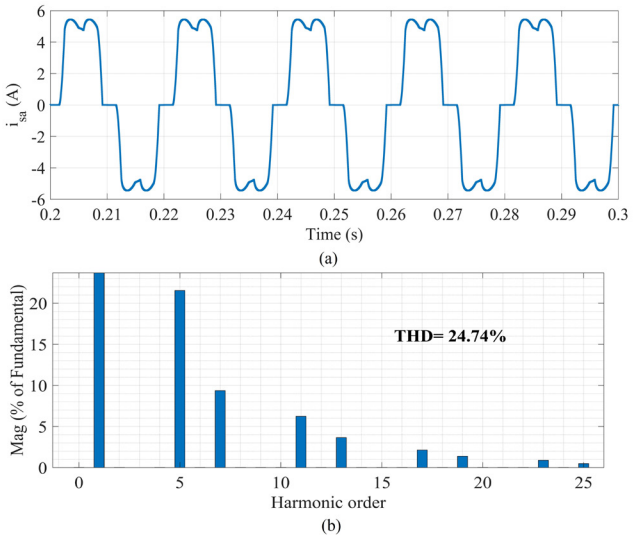


**Fig. 6** Simulation results before harmonic mitigation; (a) Source current; (b) Harmonic spectrum

injection. Fig. 7 illustrates the balanced source voltages and current, the load current, and the filter current, respectively. After inserting the filter at 0.1 [s], the source current waveform appears purely sinusoidal and in phase with the grid voltage. The waveform of the DC bus voltage is shown in Fig. 8, where the reference is reached at 21.58 [ms].

The waveforms that describe the behaviors of active and reactive power are shown in Fig. 9. The results demonstrate

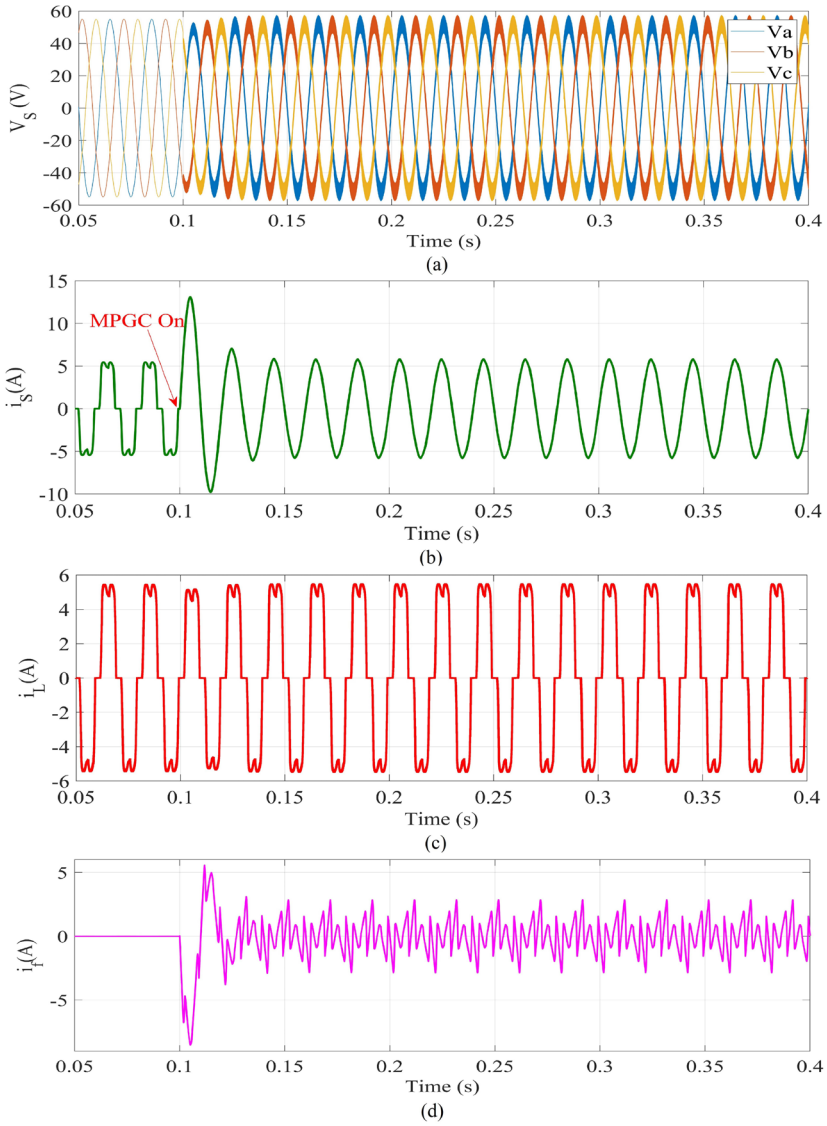


**Fig. 7** Simulation results after inserting MPGC with 0 W/m$^2$; (a) PCC voltage; (b) Source current; (c) Load current; (d) Inverter current

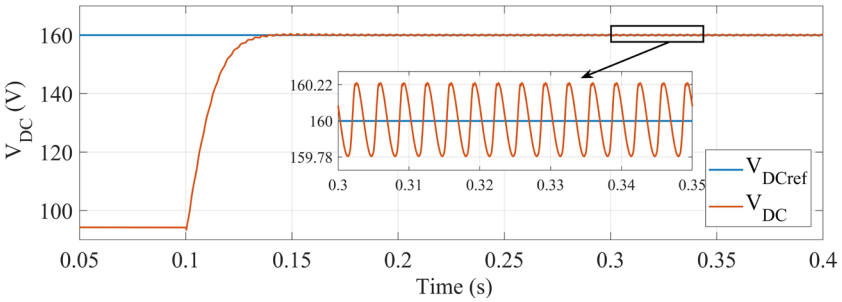


**Fig. 8** The DC bus voltage simulation result (0 W/m$^2$)

the effectiveness of the proposed controller, as the two references are tracked quickly. Whereas the reactive power is approximately equal to zero, this result indicates the unity power factor. On the other hand, the power ripple is reduced compared to a PI controller, as shown in Fig. 9 (b) and (c).

The spectrum analysis of the source current after inserting the MPGC has been illustrated in Fig. 10. The total harmonic distortion (THD) is reduced from 24.83% to 1.76% using the PI controller and 0.96% using the GWO-BS controller, which meets the IEEE 519-2014 standard [32] and confirms the excellent performance of the GWO-BS.

The MPGC-based GWO-BS controller investigated a load perturbation condition where the load resistance changed at $t = 0.2$ [s] from $R_L = 16$ [Ω] to $R_L = 12$ [Ω] and vice

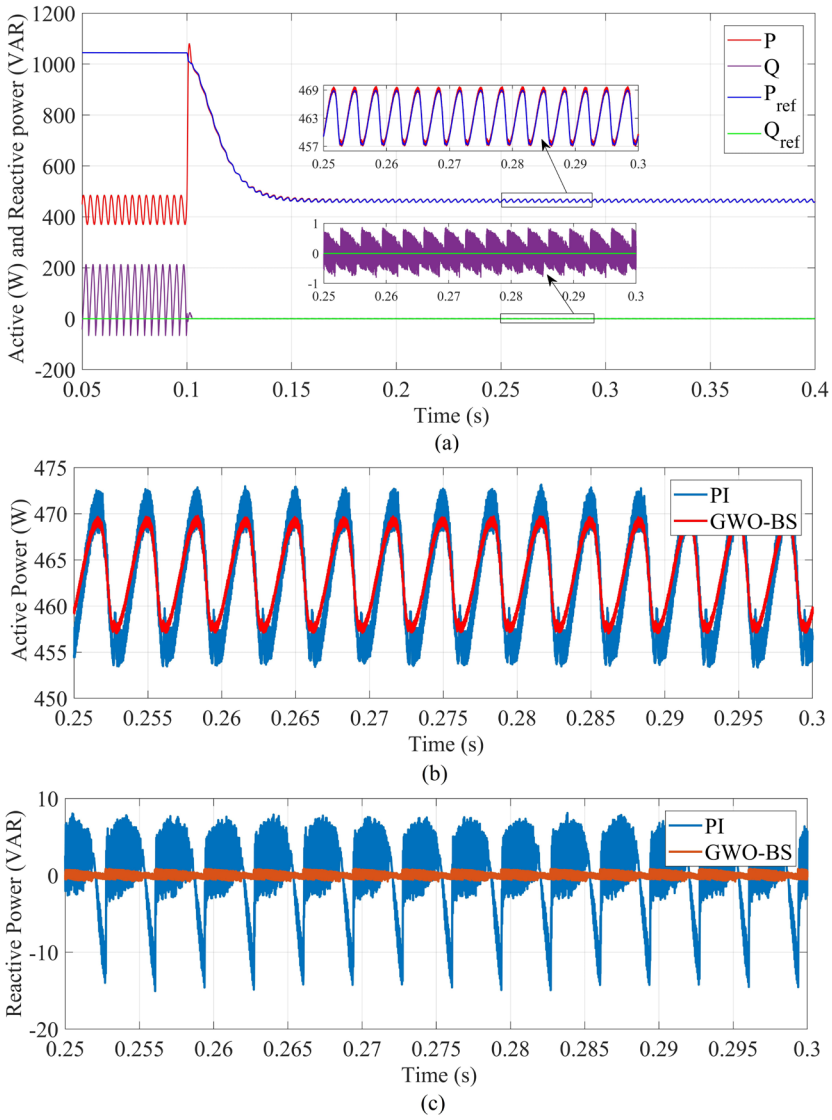


**Fig. 9** Simulation results of the active and reactive power behavior before and after inserting the MPGC (0 W/m²); (a) Active and reactive power; (b) Active power zoom; (c) Reactive power zoom

versa at $t = 0.3$ [s]. The simulation results show that the filter rejects the disturbance in which the DC bus voltage quickly recovers its reference after a load change occurs. The active power reference is rapidly tracked, as shown in Fig. 11.

The simulation results obtained after inserting the PV panels are shown in Fig. 12. Before inserting the PV panels, the nonlinear load was supplied with the necessary power using only the grid and the MPGC. After inserting the PV panels at $t = 0.2$ [s], the PV panels inject the energy generated into the grid, which reduces the source current generated, as shown in Fig. 12 (a). When solar irradiation increased, the source current decreased. In $t = 0.4$ [s], the source current has become negative due to the power of the PV panels, which has become higher than the load power demand. The DC bus voltage behavior during the PV panels injection is depicted in Fig. 12 (b). The DC bus voltage shows a reduced overshoot when inserting the PV panels, but it quickly tracks its reference.

When the irradiation varied from 200 W/m² to 400 W/m² and 400 W/m² to 1000 W/m². In Fig. 12 (c), when the PV panels launched, the active power of the source decreased. The high irradiation will increase the PV power generated, and thus the active power of the source will decrease. As previously stated, at $t = 0.4$ s, the power of the PV panels is higher than the load power, resulting in a negative source power. Throughout these tests, the source's reactive power remained close to zero.

After installing the PV panels, the source current was examined using a fast Fourier transformation. Under 200 W/m² irradiation, the THD equals 1.42% using GWO-BS. And under irradiation equal to 400 W/m², the THD for the proposed GWO-BS is 3.44%. Finally,

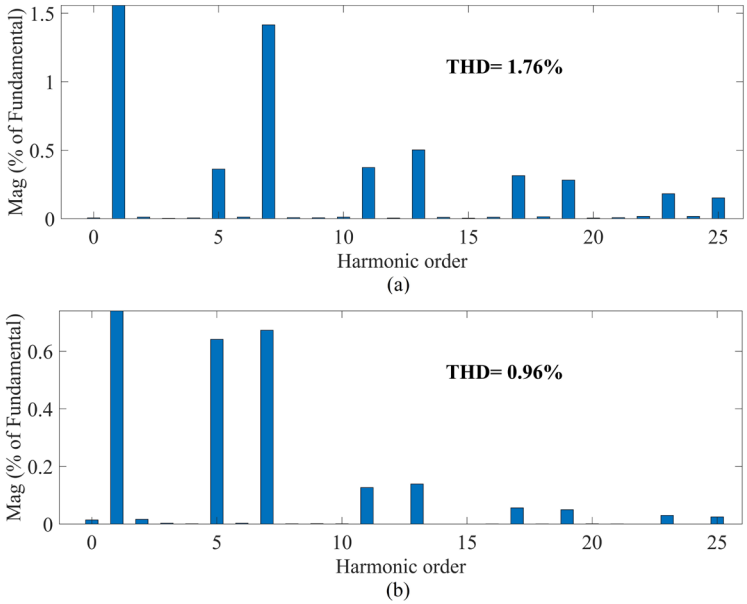


**Fig. 10** The spectrum analysis of source current using; (a) PI; (b) GWO-BS

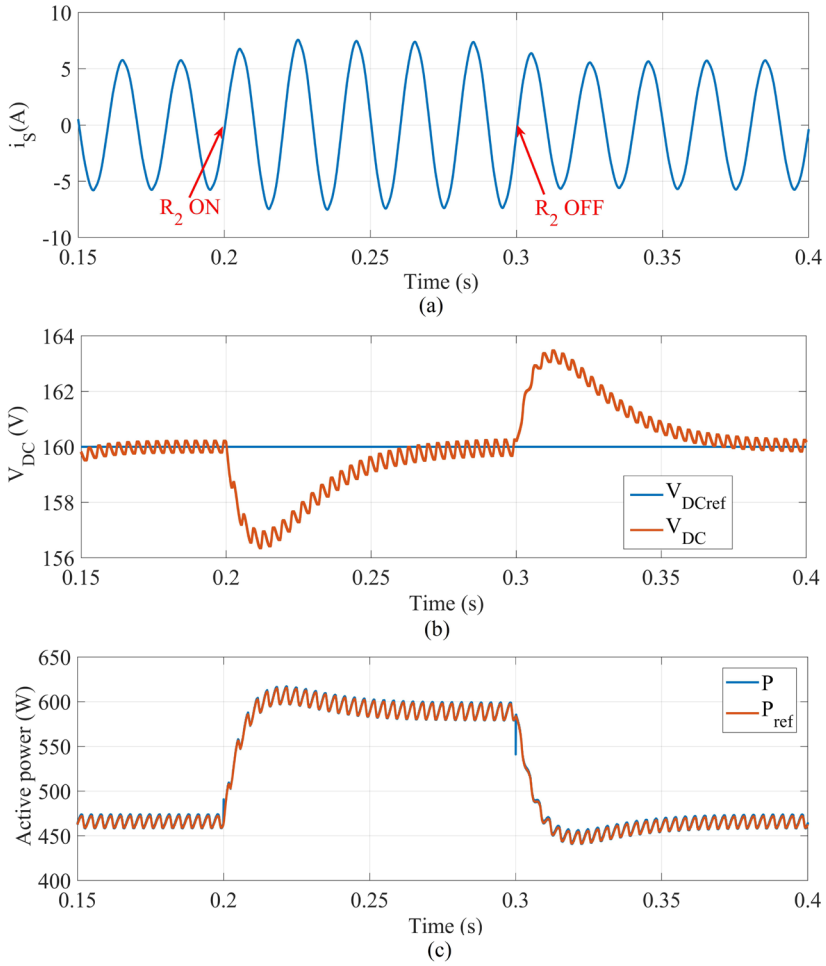


**Fig. 11** The simulation results of the MPGC behavior under load variation; (a) Source current; (b) DC bus voltage; (c) Active power

the THD for irradiation equal to 1000 W/m$^2$ is 2.34%. In Table 3, a comparison has been performed to compare the proposed controller with the PI controller.

## 5 Conclusions

This paper investigates fixed switching direct power control-based back-stepping controller optimized thanks to

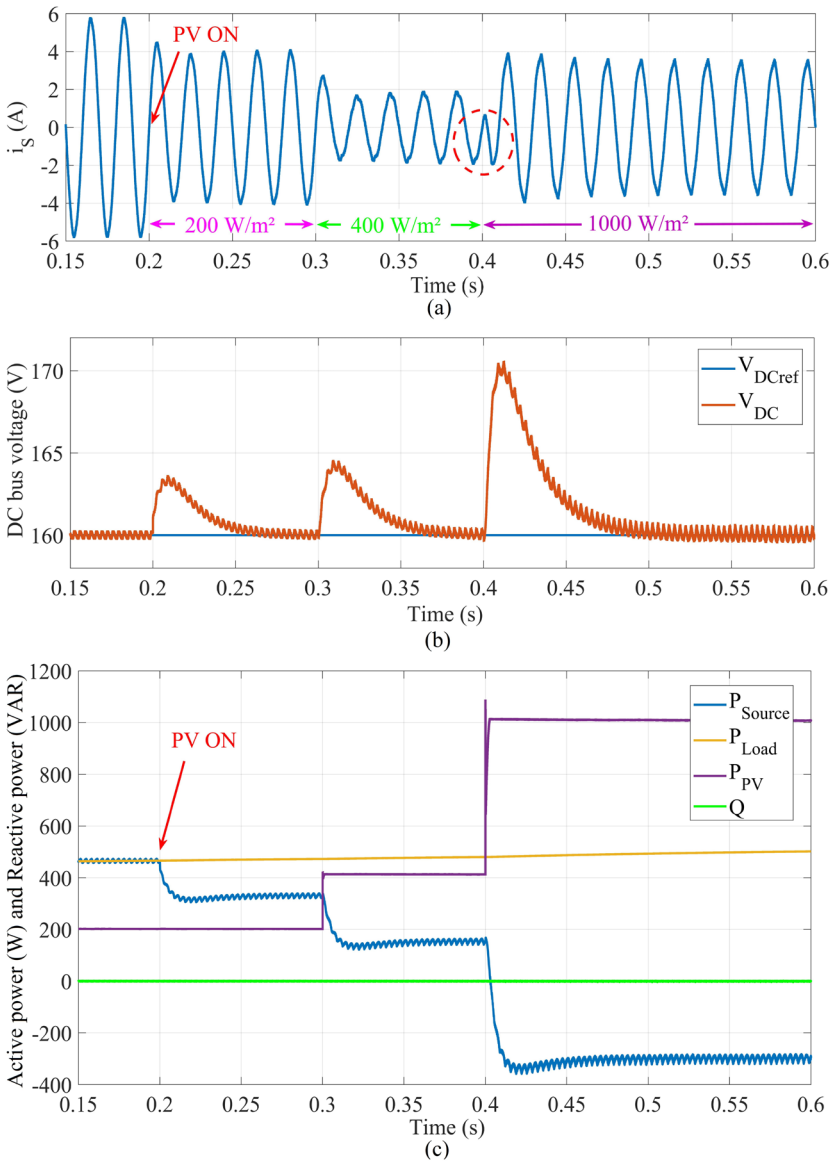


**Fig. 12** The simulation results of the PV Grid-connected system before connecting the PV panels and after coupling it; (a) Source current; (b) DC bus voltage; (c) Active and reactive power

**Table 3** Comparative study of DPC-GWOBS and DPC-PI

| Controller | Settling time [ms] | Overshoot (%) | Power ripple (w) | ITAE | THD% (0 W/m²) | THD% (200 W/m²) | THD% (400 W/m²) | THD% (1000 W/m²) |
|---|---|---|---|---|---|---|---|---|
| DPC- PI | 25.74 | 4.2 | 20.05 | 0.1511 | 1.76 | 2.4 | 4.74 | 3.79 |
| DPC-GWOBS | 21.58 | 0 | 12.60 | 0.1299 | 0.96 | 1.42 | 3.44 | 2.34 |

the GWO algorithm for interleaved boost converter-based MPGC systems. MATLAB/Simulink simulation results confirm the proposed configuration's performance and evidence of its effectiveness as a solution for PV power injection in the grid, current harmonics mitigation, and reactive power compensation. The source current's total harmonic distortion (THD) was minimized from 24.74% to 0.96% to satisfy the IEEE 519-2014 standard [32], and the unit power factor was reached due to the reactive power compensation strategy. The results show the response of the proposed system under changing load, where disturbances are rejected quickly. After inserting the PV panels through the IBC, the active power generated by the source is decreased. The obtained THDs of source current while injecting the PV power are 1.42%, 3.44%, and 2.34% for 200 W/m², 400 W/m², and 1000 W/m² of solar radiation, respectively.

Those results demonstrate the effectiveness of the GWO-BS. Moreover, the proposed scheme can operate under changing climatic conditions. Therefore, the system investigated can mitigate the current harmonics, reactive power cancellation, and PV power injection with less THD and power ripple.

**Acknowledgement**

This work is a part of both PRFU projects N° A01L07UN340120190001 supported by the University of Bordj Bou Arreridj, and N° A01LO7UN280120220005 supported by the University of Msila.

## References

[1] Molina, M. G., Espejo, E. J. "Modeling and simulation of grid-connected photovoltaic energy conversion systems", International Journal of Hydrogen Energy, 39(16), pp. 8702–8707, 2014. https://doi.org/10.1016/j.ijhydene.2013.12.048

[2] Chelli, Z., Lakehal, A., Khoualdia, T., Djeghader, Y. "Study on Shunt Active Power Filter Control Strategies of Three-phase Grid-connected Photovoltaic Systems", Periodica Polytechnica Electrical Engineering and Computer Science, 63(3), pp. 213–226, 2019. https://doi.org/10.3311/PPee.14025

[3] Liang, X., Andalib-Bin-Karim, C. "Harmonics and Mitigation Techniques Through Advanced Control in Grid-Connected Renewable Energy Sources: A Review", IEEE Transactions on Industry Applications, 54(4), pp. 3100–3111, 2018. https://doi.org/10.1109/TIA.2018.2823680

[4] Barghi Latran, M., Teke, A. "Investigation of multilevel multifunctional grid connected inverter topologies and control strategies used in photovoltaic systems", Renewable and Sustainable Energy Reviews, 42, pp. 361–376, 2015. https://doi.org/10.1016/j.rser.2014.10.030

[5] Aouadi, C., Abouloifa, A., Aourir, M., Lachkar, I., Tighazouane, B., Boussairi, Y. "Nonlinear Control of Double Stage Three-phase Grid-Connected Photovoltaic Systems", IFAC-PapersOnLine, 55(12), pp. 526–531, 2022. https://doi.org/10.1016/j.ifacol.2022.07.365

[6] Ouai, A., Mokrani, L., Machmoum, M., Houari, A. "Power Quality Improvement of a Solar Energy Conversion System by a Coordinated Active and LCL Filtering", Periodica Polytechnica Electrical Engineering and Computer Science, 65(4), pp. 373–381, 2021. https://doi.org/10.3311/PPee.17215

[7] Saidj, S. H., Boumechta, S., Degla, A., Djoudi, A., Arab, A. H., Haddadi, M. "Comparison and Experimental Tests between Conventional and Interleaved DC/DC Boost Converter Topology", In: 2020 6th International Symposium on New and Renewable Energy (SIENR), Ghadaia, Algeria, 2021, pp. 1–5. ISBN 978-1-7281-9578-0 https://doi.org/10.1109/SIENR50924.2021.9631894

[8] Soumana, R. A., Saulo, M. J., Muriithi, C. M. "New control strategy for multifunctional grid-connected photovoltaic systems", Results in Engineering, 14, 100422, 2022. https://doi.org/10.1016/j.rineng.2022.100422

[9] Malinowski, M., Jasinski, M., Kazmierkowski, M. P. "Simple Direct Power Control of Three-Phase PWM Rectifier Using Space-Vector Modulation (DPC-SVM)", IEEE Transactions on Industrial Electronics, 51(2), pp. 447–454, 2004. https://doi.org/10.1109/TIE.2004.825278

[10] Chettibi, N., Mellit, A. "PSO based Direct Power Control of grid connected photovoltaic system", In: 2015 4th International Conference on Electrical Engineering (ICEE), Boumerdes, Algeria, 2015, pp. 1–6. ISBN 978-1-4673-6673-1 https://doi.org/10.1109/INTEE.2015.7416732

[11] Azad, A. H., Shateri, H., Dragičević, T., Zhang, C. "A Novel Robust Control Strategy For Grid-Connected PV Systems Based On Modified Direct Power Control", In: 2021 IEEE International Conference on Predictive Control of Electrical Drives and Power Electronics (PRECEDE), Jinan, China, 2021, pp. 753–758. ISBN 978-1-6654-2558-2 https://doi.org/10.1109/PRECEDE51386.2021.9681016

[12] Zeghdi, Z., Barazane, L., Bekakra, Y., Larabi, A. "Improved Backstepping Control of a DFIG based Wind Energy Conversion System using Ant Lion Optimizer Algorithm", Periodica Polytechnica Electrical Engineering and Computer Science, 66(1), pp. 43–59, 2022. https://doi.org/10.3311/PPee.18716

[13] Chebabhi, A., Al-dwa, A. A. M., Barkat, S., Zebiri, F., "Backstepping control of a grid-connected four-leg PWM rectifier under both balanced and unbalanced grid conditions", International Journal of System Assurance Engineering and Management, 14(1), pp. 1–18, 2023. https://doi.org/10.1007/s13198-022-01826-8

[14] Khadar, S., Kouzou, A., Rezzaoui, M. M., Hafaifa, A. "Sensorless Control Technique of Open-End Winding Five Phase Induction Motor under Partial Stator Winding Short-Circuit", Periodica Polytechnica Electrical Engineering and Computer Science, 64(1), pp. 2–19, 2020. https://doi.org/10.3311/PPee.14306

[15] Chebabhi, A., Fellah, M. K., Kessal, A., Benkhoris, M. F. "Comparative study of reference currents and DC bus voltage control for Three-Phase Four-Wire Four-Leg SAPF to compensate harmonics and reactive power with 3D SVM", ISA Transactions, 57, pp. 360–372, 2015. https://doi.org/10.1016/j.isatra.2015.01.011

[16] Naghmash, Armghan, H., Ahmad, I., Armghan, A., Khan, S., Arsalan, M. "Backstepping based non-linear control for maximum power point tracking in photovoltaic system", Solar Energy, 159, pp. 134–141, 2018. https://doi.org/10.1016/j.solener.2017.10.062

[17] Martin, A. D., Cano, J. M., Silva, J. F. A., Vázquez, J. R. "Backstepping control of smart grid-connected distributed photovoltaic power supplies for telecom equipment", IEEE Transactions on Energy Conversion, 30(4), pp. 1496–1504, 2015. https://doi.org/10.1109/TEC.2015.2431613

[18] Hao, X., Salhi, I., Laghrouche, S., Ait-Amirat, Y., Djerdir, A. "Backstepping Supertwisting Control of Four-Phase Interleaved Boost Converter for PEM Fuel Cell", IEEE Transactions on Power Electronics, 37(7), pp. 7858–7870, 2022. https://doi.org/10.1109/TPEL.2022.3149099

[19] Youcefa, B. E., Massoum, A., Barkat, S., Wira, P. "Backstepping Direct Power Control for Power Quality Enhancement of Grid-connected Photovoltaic System Implemented with PIL Co-simulation Technique", Advances in Modelling and Analysis C, 74(1), pp. 1–14, 2019.
https://doi.org/10.18280/ama_c.740101

[20] Daia Eddine, O. M. C., Chebabhi, A., Kessal, A. "Four leg Interleaved DC/DC boost Converter based PV system using PSO Algorithm based PI controller", In: 2022 19th International Multi-Conference on Systems, Signals & Devices (SSD), Sétif, Algeria, 2022, pp. 1415–1421. ISBN 978-1-6654-7109-1.
https://doi.org/10.1109/SSD54932.2022.9955647

[21] Daia Eddine, O. M. C., Chebabhi, A., Kessal, A., Benkhoris, M. F., Defdaf, M. "Super-Twisting Sliding Mode Control of Interleaved Boost Converter Based Photovoltaic Applications", In: 2022 International Conference of Advanced Technology in Electronic and Electrical Engineering (ICATEEE), M'sila, Algeria, 2022, pp. 1–5. ISBN 979-8-3503-4675-6
https://doi.org/10.1109/ICATEEE57445.2022.10093715

[22] Al-Dwa, A. A. M., Chebabhi, A., Defdaf, M., Guessabi, A. "New Modeling and Improved Current Control Strategy to Eliminate the Impact of Synchronization Method and Parks Transformation for Grid-connected Four-leg PWM Inverter", Periodica Polytechnica Electrical Engineering and Computer Science, 67(2), pp. 204–215, 2023.
https://doi.org/10.3311/PPee.20517

[23] Krama, A., Zellouma, L., Rabhi, B., Refaat, S. S., Bouzidi, M. "Real-time implementation of high performance control scheme for grid-tied PV system for power quality enhancement based on MPPC-SVM optimized by PSO algorithm", Energies, 11(12), 3516, 2018.
https://doi.org/10.3390/en11123516

[24] Kermadi, M., Berkouk, E. M. "Artificial intelligence-based maximum power point tracking controllers for Photovoltaic systems: Comparative study", Renewable and Sustainable Energy Reviews, 69, pp. 369–386, 2017.
https://doi.org/10.1016/j.rser.2016.11.125

[25] Obeidi, N., Kermadi, M., Belmadani, B., Allag, A., Achour, L., Mesbahi, N., Mekhilef, S. "A modified current sensorless approach for maximum power point tracking of partially shaded photovoltaic systems", Energy, 263, 125618, 2023.
https://doi.org/10.1016/j.energy.2022.125618

[26] Pilakkat, D., Kanthalakshmi, S. "An improved P&O algorithm integrated with artificial bee colony for photovoltaic systems under partial shading conditions", Solar Energy, 178, pp. 37–47, 2019.
https://doi.org/10.1016/j.solener.2018.12.008

[27] Alik, R., Jusoh, A. "An enhanced P&O checking algorithm MPPT for high tracking efficiency of partially shaded PV module", Solar Energy, 163, pp. 570–580, 2018.
https://doi.org/10.1016/j.solener.2017.12.050

[28] Mirjalili, S., Mirjalili, S. M., Lewis, A. "Grey Wolf Optimizer", Advances in Engineering Software, 69, pp. 46–61, 2014.
https://doi.org/10.1016/j.advengsoft.2013.12.007

[29] Bekakra, Y., Zellouma, L., Malik, O. "Improved predictive direct power control of shunt active power filter using GWO and ALO – Simulation and experimental study", Ain Shams Engineering Journal, 12(4), pp. 3859–3877, 2021.
https://doi.org/10.1016/j.asej.2021.04.028

[30] Muro, C., Escobedo, R., Spector, L., Coppinger, R. P. "Wolf-pack (Canis lupus) hunting strategies emerge from simple rules in computational simulations", Behavioural Processes, 88(3), pp. 192–197, 2011.
https://doi.org/10.1016/j.beproc.2011.09.006

[31] The MathWorks Inc. "MATLAB/Simulink, (9.0)", Available at: https://www.mathworks.com/products/simulink.html [Accessed: 16 April 2023]

[32] IEEE Standards Association "519-2014 IEEE Recommended Practice and Requirements for Harmonic Control in Electric Power Systems", IEEE Standards Association, Piscataway, NJ, USA, 2014.
https://doi.org/10.1109/IEEESTD.2014.6826459